water

MDPI

Article

Simulation of Internal Flow Characteristics of an Axial Flow Pump with Variable Tip Clearance

Jiantao Shen [1], Fengyang Xu [2], Li Cheng [1,*], Weifeng Pan [3], Yi Ge [4], Jiaxu Li [1] and Jiali Zhang [4]

[1] College of Hydraulic Science and Engineering, Yangzhou University, Yangzhou 214000, China; shenjiantao888@163.com (J.S.); lijiaxu_yzu@163.com (J.L.)
[2] Jiangsu Zhenjiang Jianbi Pumping Station Management Office, Zhenjiang 212006, China; xufengyang06@163.com
[3] Luoyun Water Conservancy Project Management Divison in Jiangsu Province, Suqian 223800, China; jssqpwf@163.com
[4] Jurong Water Conservancy Bureau in Jiangsu Province, Jurong 212499, China; geyi1988@126.com (Y.G.); jrfxfh@126.com (J.Z.)
* Correspondence: chengli@yzu.edu.cn

Abstract: This study investigated the influence of the change in blade tip clearance on the internal flow characteristics of a vertical axial flow pump. Taking the actual running vertical axial flow pump of a pumping station as the research object, based on the SST k-ω turbulent flow model, the numerical simulation technology was used to study the effects of different tip clearances on the pressure, turbulent kinetic energy, Z–X section pressure and flow state of the impeller at the middle section. Furthermore, the impact of clearance layer tip leakage was also analyzed. Unsteady calculations of flow characteristics under the design conditions were performed. The research results showed that the variation trend of the pressure in the impeller was basically the same under different tip clearance values. With the increase in the clearance value, the pressure gradient along the water inlet direction of the blade decreased and the leakage vorticity increased. Observing the leakage vorticity distribution of the gap layer under the flow condition of $0.6Q_0$, it was found that when the tip clearance was smaller than 1 mm, the leakage flow was small and easily assimilated by the mainstream, and the leakage flow and mainstream had a certain ability to compete, which caused adverse effects on the performance of the pump device. The pressure pulsation characteristics showed that the leakage flow caused by the tip clearance caused a high-frequency distribution, and the clearance obviously influenced the pressure pulsation characteristics.

Keywords: tip clearance; vertical axial flow pump; whole channel numerical simulation; pressure pulsation; leakage vortex

Citation: Shen, J.; Xu, F.; Cheng, L.; Pan, W.; Ge, Y.; Li, J.; Zhang, J. Simulation of Internal Flow Characteristics of an Axial Flow Pump with Variable Tip Clearance. *Water* **2022**, *14*, 1652. https://doi.org/10.3390/w14101652

Academic Editors: Ran Tao, Changliang Ye and Xijie Song

Received: 19 April 2022
Accepted: 20 May 2022
Published: 22 May 2022

1. Introduction

In the areas along the rivers in China, in order to meet the requirements of water transfer and irrigation, there are many vertical axial flow pumping stations [1,2]. These axial flow pumping stations have the characteristics of large flow and low lift [3], have been widely used in the eastern route of the South-to-North Water Diversion Project, and have achieved great social and economic benefits [4]. In the design of the vertical axial flow pump, due to the way water is pumped [5] and in order to prevent the impeller from scraping and colliding with the pump casing when the impeller rotates at high speed, it is necessary to leave a certain gap between the top of the impeller blade and the pump casing, which is the tip clearance. When the impeller is working, there is a pressure difference between the working surface and the back of the blade, and the existence of the pressure difference will lead to the generation of a leakage flow at the clearance position at the top of the blade. The interaction between the leakage flow and the main flow not only affects

the pump performance but also induces abnormal vibration and noise, and even causes safety hazards and affects the normal operation of the pumping station [6].

Domestic and foreign experts and scholars studied the influence of tip clearance flow laws and the performance of impeller machinery. Zhang Desheng et al. [7] studied the pressure difference distribution, leakage, tip leakage vortex intensity and inlet axial velocity distribution in the tip clearance area of an inclined flow pump under different tip clearances. Shi Weidong et al. [8] used the SMPLEC algorithm to simulate different clearances under different working conditions and analyzed the axial velocity and circulation distribution of an impeller outlet in detail. Zhang et al. [9] revealed the gap flow field structure and leakage vortex evolution of a semi-open centrifugal pump by changing the gap according to the numerical calculation of the whole flow channel of the semi-open impeller centrifugal pump. Li Hui et al. [10] used the delayed detached vortex method to simulate a dynamic blade with a tip clearance and then studied the turbulent characteristics of the leakage area through the turbulent kinetic energy distribution and Lumley triangle. Then, the POD decomposition method was used to decompose the flow field in the leakage area, and finally, the loss analysis of the tip leakage flow was carried out. Lu Jinling et al. [11] carried out a full flow channel numerical simulation of a semi-open centrifugal pump using Fourier transform (FFT) to convert the time domain value of each monitoring point to a frequency domain value and analyzed the correlation mechanism between leakage vortex trajectory and blade load, as well as the spectral characteristics of the leakage vortex. Li et al. [12] studied the internal flow characteristics of the tip clearance of tubular turbines under off-design conditions and analyzed the pressure and velocity vector distribution of the internal flow field in the tip clearance, as well as the axial velocity and turbulent kinetic energy distribution characteristics in the tip clearance. Liu et al. [13] observed the development and trajectory of the leakage vortex by changing the tip clearance and performed a spectral analysis. When the tip clearance increased from 0 mm to 10 mm, the maximum amplitude of the pressure pulsation in the impeller increased sharply. Due to the increase in leakage flow, the main frequency increased from 145 Hz to 184 Hz. Kan et al. [14] used a standard k-epsilon turbulence model to simulate the flow characteristics of a self-developed helical axial flow pump. Pressure, streamline and turbulent kinetic energy analyses of the leakage flow (TLF) in a helical axial flow pump were undertaken, revealing the effect of tip clearance on the flow behavior and boosting performance of a helical axial flow pump. Shen et al. [15] used a computational fluid dynamics method to study the effect of different tip clearance widths on the tip flow dynamics and main flow characteristics of axial flow pumps. The distribution 0.7Q (BEP) of turbulent kinetic energy, average axial velocity and average vorticity at a specific flow rate was analyzed, and it was found that the flow structure of the tip vortex and its transmission strongly depended on the tip gap width. The efficiency and head of the pump both increase the energy loss as the tip clearance increases. Feng Jianjun et al. [16] studied the pressure pulsation of an axial flow pump under different tip clearances and proposed a new method to determine the pressure pulsation of the grid node in a pump based on pressure statistics. It was found that the existence of a tip clearance enlarged the pressure pulsation from the hub to the rim of the impeller. Li Yibin et al. [17] studied the pressure pulsation characteristics of different tip clearance regions of a diagonal flow pump under the condition of a small flow rate, and the influence on the transient operation stability of the diagonal flow pump was revealed. Through the analysis of the pressure pulsation spectrum, the internal relationship between the R_{TC} and the pressure pulsation in the vicinity of the tip clearance area was understood. The results show that selecting an appropriately small R_{TC} can improve the overall hydraulic performance of the oblique flow pump. Zhang Hua et al. [18] studied the influence degree and mechanism of the blade tip clearance on the internal and external characteristics of the centrifugal pump, a special adjustment mechanism for the blade tip clearance was designed, and the external characteristics test and a pressure pulsation test were carried out at the same time. The results show that the ratio of the tip clearance to the average diameter of the impeller should be between 0.13% and 0.22%. This provides

a reference for the vibration and noise reduction of a semi-open screw centrifugal pump. Li Rennian et al. [19] studied the influence of the tip clearance on the inlet pressure pulsation characteristics of the diagonal flow pump, where the results show that with the increase of the tip clearance, the lift of the diagonal flow pump decreases gradually. The amplitude of pressure pulsation in the mainstream area of the impeller inlet is small, while the amplitude of pressure pulsation in the near-wall area is large. The larger tip clearance can reduce the pressure pulsation amplitude at the impeller inlet, which is beneficial for improving the operation stability of the model oblique flow pump. Li Yaojun et al. [20] studied the unsteady flow characteristics of the axial flow pump rim area under different tip clearances, where the results showed that when the tip clearance increased from $0.001D_2$ to $0.003D_2$, the pump head and efficiency decreased by 6.2% and 5.6%, respectively. When the clearance value is greater than $0.001D_2$, the primary leakage vortex in the rim clearance developed to the front face of the adjacent blade and a large number of secondary leakage vortices are generated in the clearance area. Guelich, J. and Ulanicki, B. et al. [21,22] studied the efficiency and power characteristics of a pump group, which were simulated by changing the Reynolds number and considering the constant or variable speed of the pump.

In this study, a full flow channel numerical calculations were carried out for the vertical axial flow pump [23], and the influence of the tip clearance change on the total pressure, turbulent kinetic energy distribution, Z–X section pressure, flow state, and the leakage flow and leakage volume of the gap layer were analyzed in detail. Numerical simulations of the unsteady flow in the axial flow pump with different tip clearance sizes were carried out to study the effect of the clearance size on the leakage vortex shape of the rim clearance and to analyze the pressure pulsation characteristics of the clearance layer to obtain the optimal blade rim. The variation law of the side and inlet and outlet pressure pulsations with different rim gap sizes theoretically revealed the gap flow field structure and leakage flow evolution of the vertical axial flow pump with a changing gap. This provides reference significance for more efficient operation and management of vertical axial flow pump stations [24,25].

2. Numeral Calculations

2.1. Vertical Axial Flow Pump Parameters and Research Plan

This study took a vertical bidirectional axial flow pump station as the prototype for the 3D modeling. The pump station adopted the 2500ZLQ-20-3.0 vertical axis open axial flow pump produced by a factory. The designed flow rate of the pump was Q_0 = 20 m^3/s, the impeller diameter was 2.50 m, the number of impeller blades was 3, the number of guide blades was 7, the specific speed was 1250 and the impeller speed was 150 r/min.

In order to study the change in the internal flow characteristics of the pump under different clearance sizes and to ensure that the external characteristics of the prototype pump remained unchanged, the method of turning the impeller was adopted [26]. Four different tip clearances (d = 1 mm, 2.5 mm, 3.5 mm, 5 mm) were selected to simulate the flow under five working conditions. Through comparative analysis, the internal flow of vertical axial flow pump with different tip clearances was expounded. Figure 1a below is the flow chart of the research plan. Figure 1b is the tip clearance diagram of the vertical axial flow pump.

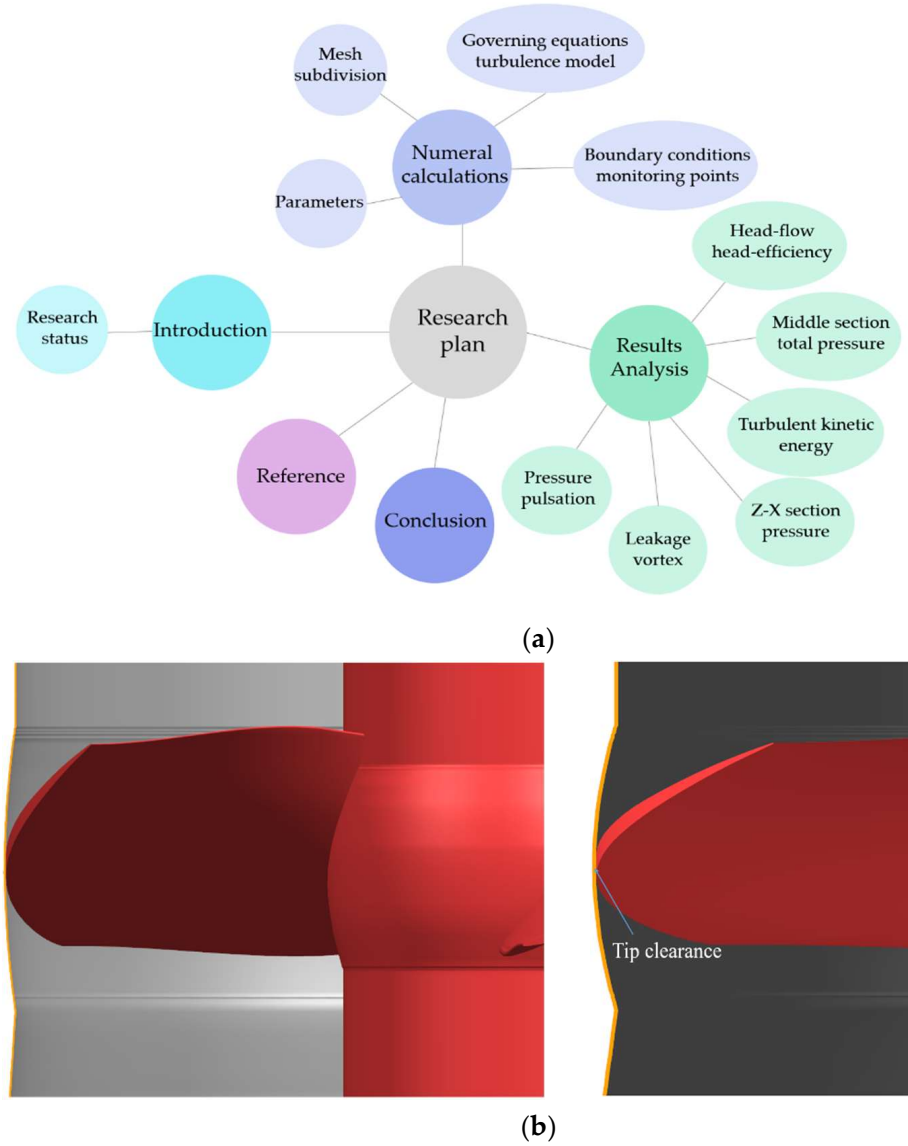

Figure 1. (**a**) Research program flow chart. (**b**) Three-dimensional schematic diagram of the tip clearance.

2.2. Mesh Subdivision

As shown in Figure 2a, the physical model of the computational domain in this study included the inlet section, the impeller section, the guide vane section and the outlet section. Considering the control of the overall number of mesh elements and the number of effective nodes, a hexahedral mesh was used for the divisions and the impeller section was refined to control the mesh quality.

Since the mesh size and quality have an important influence on the calculation results, by adjusting the mesh size of the impeller blade surface and the rim clearance area, the design flow conditions of the pump under different mesh schemes when the tip clearance was d = 2.5 mm were compared. The efficiency of the pump was compared with the test results, and a mesh-independent analysis was conducted. As shown in Table 1, the pump head and efficiency calculated using grid schemes A, B and C were basically the same. Considering the economy of numerical calculation, grid scheme B was adopted in this study. With different tip clearances, the total number of computational domain grids was about 1.3×10^7; the global mesh and impeller vane mesh are shown in Figure 2b.

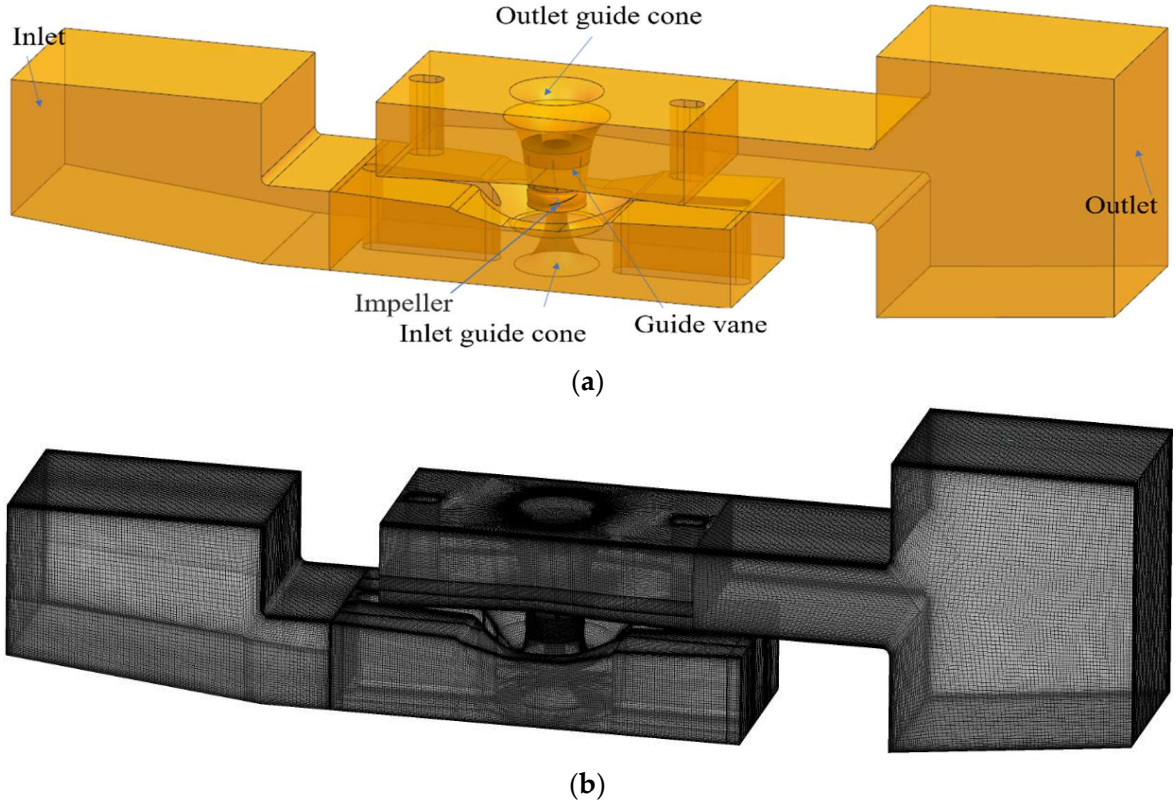

Figure 2. (**a**) Computational fluid domain of the whole channel. (**b**) Global grid.

Table 1. Grid independence.

Plan	Total Number of Grids	Efficiency Test Value /%	Efficiency Calculated Value /%	Efficiency Relative Error /%	Head Test Value /m	Head Calculated Value/m	Head Relative Error /m
A	10,697,069	61.61	64.25	4.29	1.90	1.9283	2.79
B	13,422,014	61.61	63.72	3.42	1.90	1.9003	1.31
C	15,342,176	61.61	63.34	2.81	1.90	1.8916	0.83

2.3. Governing Equations and Turbulence Model Selection

The internal flow of a pump is unsteady viscous flow, which can be described using Navier–Stokes equations [27]. The Reynolds-averaged Navier–Stokes (RANS) method was used to decompose the various characteristic variables of the turbulent flow into time-averaged Reynolds equations and fluctuating values, and then the turbulent viscosity coefficient was introduced to establish the turbulent model. For a general incompressible Newtonian fluid, the following control equations are used.

The mass conservation equation, also called the continuity equation, is as follows:

$$\frac{\partial \rho_f}{\partial t} + \nabla \cdot \left(\rho_f v\right) = 0$$

Momentum equation:

$$\frac{\partial \rho_f v}{\partial t} + \nabla \cdot \left(\rho_f vv - \tau_f\right) = f_f$$

where t is time, f_f is the volume force vector, ρ_f is the fluid density, v is the fluid velocity vector and τ_f is the shear force tensor given by

$$\tau_f = (-p + \mu \nabla \cdot v)I + 2\mu e$$

where p is the static pressure, μ is the dynamic viscosity and e is the velocity stress tensor:

$$e = \left(\nabla v + \nabla v^T\right)$$

The numerical simulation and experimental results showed that under the optimal conditions, the predicted external characteristic curve of the SST k-ω turbulence model was in good agreement with the experimental curve, where the head error was 4.688% [28]. Therefore, the SST k–ω was selected as the turbulence model to conduct the numerical simulation of the whole flow channel in the computational domain of the axial flow pump, where k is the turbulent kinetic energy, and the transport equation is:

$$\rho\frac{\partial(k)}{\partial t} + \rho\frac{\partial}{\partial x_j}(U_j k) = \frac{\partial}{\partial x_j}\left[\left(\mu + \frac{\mu_t}{\sigma_k}\right)\frac{\partial k}{\partial x_j}\right] + P_k - \beta'\rho k\omega$$

ω is the turbulent dissipation rate, and the related equation is

$$\frac{\partial(\rho\omega)}{\partial t} + \frac{\partial}{\partial x_j}(\rho U_j\omega) = \frac{\partial}{\partial x_j}\left[\left(\mu + \frac{\mu_t}{\sigma_\omega}\right)\frac{\partial\omega}{\partial x_j}\right] + \alpha\frac{\omega}{k}P_k - \beta\rho\omega^2 + 2(1-F_1)\rho\frac{1}{\sigma_{\omega 2}\omega}\frac{\partial k}{\partial x_j}\frac{\partial\omega}{\partial x_j}$$

In this formula, U_j is the vector velocity (m/s), P_k is the turbulent generation rate and μ_t is the turbulent viscosity (m^2/s).

2.4. Boundary Conditions and Arrangement of the Pressure Fluctuation Monitoring Points

The boundary conditions in this study were the velocity inlet and free outlet. The flow at the pump outlet was fully developed. The impeller speed was n = 150 r/min and the rotor–stator dynamic–static interface was a frozen rotor. The wall of each flow component adopted a smooth non-slip wall, The impeller surface and hub surface were set as moving walls without heat transfer, and the convergence accuracy was 10^{-4}. In the unsteady calculations, the time step was 1/40 of the impeller rotation period of 0.4 s, and the sampling time was 8 impeller rotation periods. Detailed parameters are shown in Table 2.

Table 2. Parameter settings for the constant and unsteady calculations.

Calculated Parameters	Settings	Calculated Parameters	Settings
Flow assumption	Incompressible	Static–static interface	GGI
Simulation type	Steady	Dynamic–static interface	Frozen rotor
Inlet boundary condition	Quality inlet	Wall condition	No slippage
Outlet boundary condition	Pressure outlet	Wall function	Scalable wall function
Impeller speed	150 r/min	Convergence accuracy	10^{-4}
Flow assumption	Incompressible	Impeller speed	150 r/min
Simulation type	Transient	Static–static interface	GGI
Time Step	0.01 s	Dynamic–static interface	Transient rotor stator
Total time	0.32 s	Wall conditions	No slippage
Inlet boundary condition	Quality inlet	Wall function	Scalable wall function
Outlet boundary Condition	Pressure outlet	Convergence accuracy	10^{-4}

In order to analyze the pressure fluctuation characteristics of a blade near the flange side, as well as the inlet and outlet, under the influence of different flange clearance leakage flow, the pressure fluctuation monitoring points were arranged as shown in Figure 3.

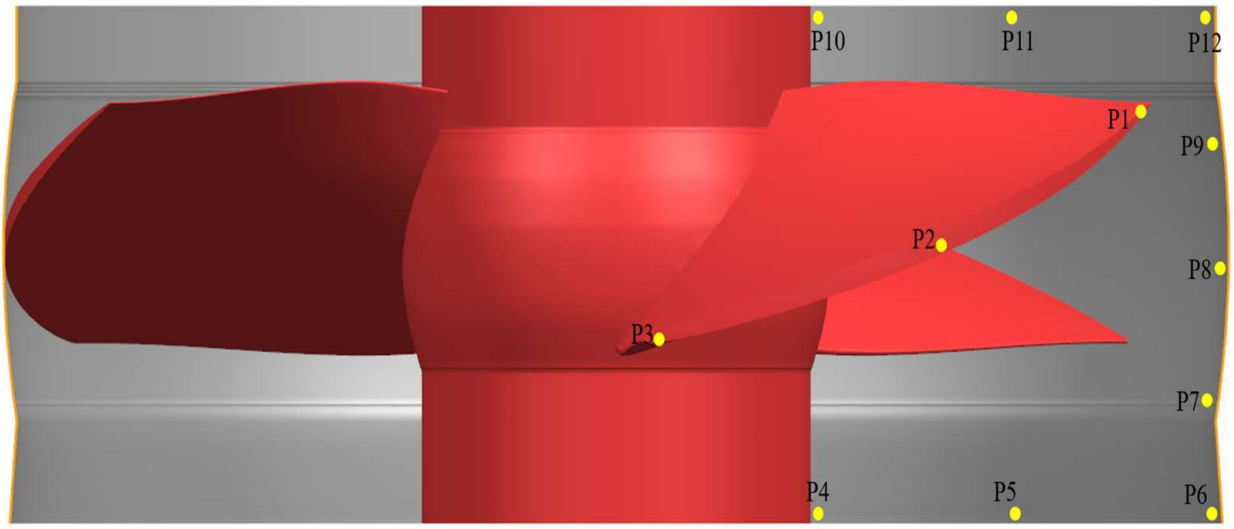

Figure 3. Schematic diagram of the monitoring point layout.

3. Calculation Results and Analysis

3.1. Head–Flow Curve and Head–Efficiency Curve

Figures 4 and 5 give the head–flow curve and the efficiency–flow curve under different clearances, respectively, where the YJ values represent the sizes of the different tip clearances in units of mm.

The test situation represented the head when the gap was 1 mm and evaluated the relationship between the efficiency and flow rate. It can be seen from Figure 4 that the test head value was generally higher than the numerical simulation head value, and decreased with the increase in the flow rate. However, when the flow rate increased, the drop rate was larger than the numerical model head, and there was a cross-over with the numerical model head value. The gap between the test and simulation was only about 0.2 m. Figure 5 shows that the efficiency of the test was lower than the simulation efficiency under the condition of a small flow rate, but the efficiency growth rate was larger than the simulation value. At $0.6Q_0$, the test efficiency gradually intersected with the simulation efficiency and began to exceed it. At $0.9Q_0$, the efficiency gap between the test and the simulation was the largest, reaching less than 2%. It shows that the efficiency gap was within the controllable range, and the numerical simulation was basically consistent with the experimental situation.

This shows that the digital–analog calculation was closer to the actual situation. It can be seen from Figure 5 that there was no linear correlation between the drop in the lift and the increase in the clearance. In the process of increasing the clearance from 1 mm to 5 mm, with the increase in the clearance, the change in the lift and efficiency was relatively small. When the gap was small, the leakage was small; the leakage was very small relative to the mainstream, and the impact on the mainstream was negligible, making the efficiency higher. It can be seen from Figure 5 that with the gradual increase in the gap, the leakage had a certain influence on the mainstream and the influence on the flow field increased, which caused the head and efficiency drops to be significantly larger. When the clearance continued to increase (referring to the 3.5 mm–5 mm stage), the leakage volume also continued to increase, but the increase in the tip clearance was moderate compared with the previous one. The difference in leakage flow was limited; therefore, the drop in the head and efficiency was also smaller than before.

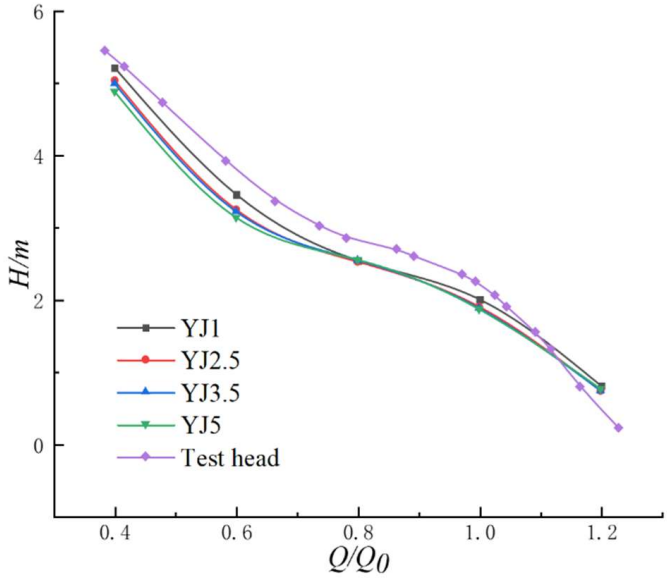

Figure 4. Head–flow curve.

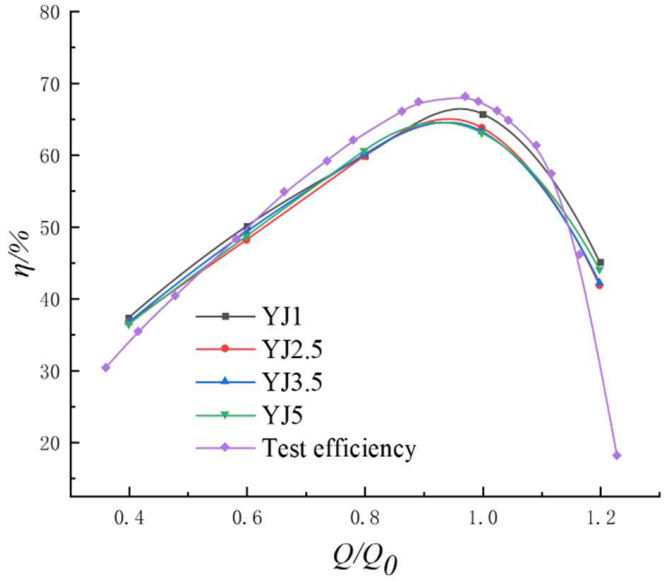

Figure 5. Efficiency–flow curve.

3.2. Effect of Clearance Variation on Total Pressure Distribution of Impeller Middle Section

Figure 6 shows the total pressure distribution of the middle section of the impeller under different tip clearances. It can be seen from Figure 6 that the pressure changed in the same trend under different tip clearances. The diffusion and the pressure at the outlet were small, and the degree of pressure diffusion was relatively uniform in this section, but at the edge of the front end of the impeller, affected by the gap leakage vortex, a local high-pressure area appeared. There were high-pressure areas on both the working face and the back of the blade, which were mainly due to the existence of the tip clearance. The high-pressure fluid on the working face of the blade passed through the tip clearance and directly acted on the back of the blade. With the increase in the clearance value, the pressure gradient along the water inlet direction of the blade decreased. As the leakage vorticity increased, the work done by the water on the blade decreased. When the tip clearance increased from 1 mm to 5 mm and the tip clearance was small, the leakage vorticity was small, and it was easier to generate a local high pressure at the edge of the inlet direction.

When the tip clearance value was large, the high-pressure fluid crossed the gap. It acted on the back of the blade, which reduced the workability of the water flow for the blade.

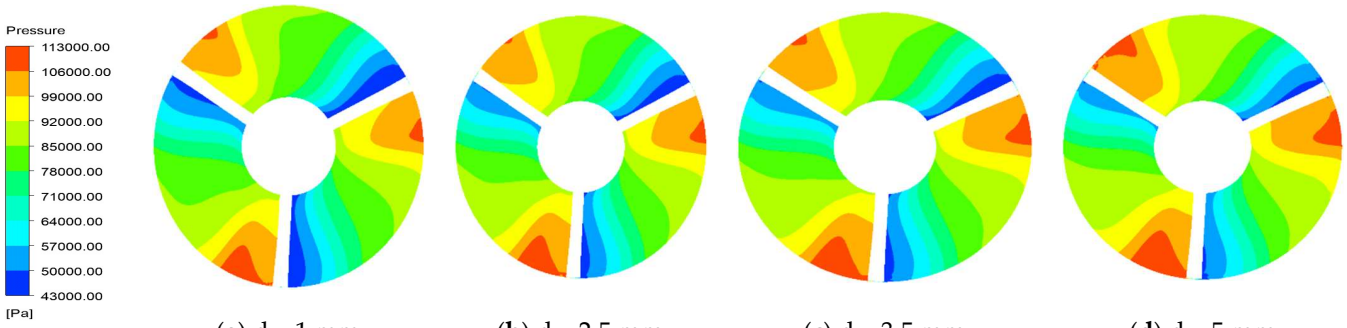

(**a**) d = 1 mm (**b**) d = 2.5 mm (**c**) d = 3.5 mm (**d**) d = 5 mm

Figure 6. Total pressure distribution of the middle section of the impeller under the design conditions.

3.3. Effect of the Clearance Variation on the Turbulent Kinetic Energy Distribution in the Middle Section of Impeller

Figure 7 shows the distribution of the turbulent kinetic energy in the middle section of the impeller under the design conditions. It can be seen from the figure that the area with a large turbulent kinetic energy was concentrated at the edge of the impeller, and the turbulent kinetic energy was particularly large near the tip of the blade. This was because the high-pressure fluid leaked from the gap and crossed the working face to the back to form a mixing loss zone. This affected the normal flow of the fluid in the flow channel, where a region of high turbulent kinetic energy was created. In the four different tip clearance cases, the tip leakage flow increased with the increase in the tip clearance size, and the extreme value of the leakage flow increased when the turbulent kinetic energy region increased. Combined with the analysis of the total pressure distribution in the middle section of the impeller in Figure 6, it can be seen that the pressure gradient in the flow channel along the water flow direction was reduced and the influence of the leakage flow changed, resulting in the formation of unstable turbulent pulsations inside the flow channel. The interaction of fluid molecules, friction and collisions aggravated the internal energy loss of the fluid such that a part of the internal energy was converted into heat energy and conducted out, thereby reducing the efficiency of the pump device.

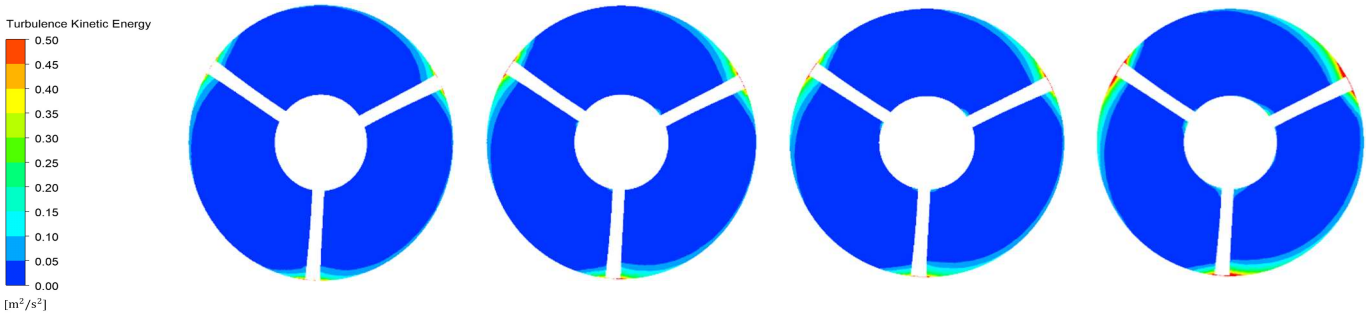

(**a**) d = 1 mm (**b**) d = 2.5 mm (**c**) d = 3.5 mm (**d**) d = 5 mm

Figure 7. Distribution of the turbulent kinetic energy in the middle section of the impeller under the design conditions.

3.4. Effect of the Gap Change on the Pressure and Flow State of the Z–X Section

Figure 8 shows the pressure distribution of Z–X section with different tip clearances under the design conditions. It can be seen that under different tip clearance values, high-pressure fluid entered from the bottom inlet, passed through the impeller guide vane in turn and flowed out from the upper outlet. The total pressure of the Z–X section increased

gradually along the inlet direction and reached the maximum at the outlet, and there was a local high-pressure area at the outlet section of the impeller. The total pressure fluctuation at the inlet position of the impeller was not obvious. When the high-pressure fluid reached the blade working face, the isobaric line began to change significantly and was accompanied by large fluctuations. The pressure fluctuations were mostly concentrated in the impeller channel, which intensified the instability of the fluid flow. It can also be seen from Figure 8 that the pressure of the blade's working face was significantly greater than that of the back surface, and even the pressure of some regions was close to zero at the back surface of the blade. This was because the high-pressure fluid near the tip clearance of the impeller blade working face side leaked to the back of the blade through the clearance, and the working efficiency of the blade was reduced, which showed the trend of pressure reduction on the back of the blade.

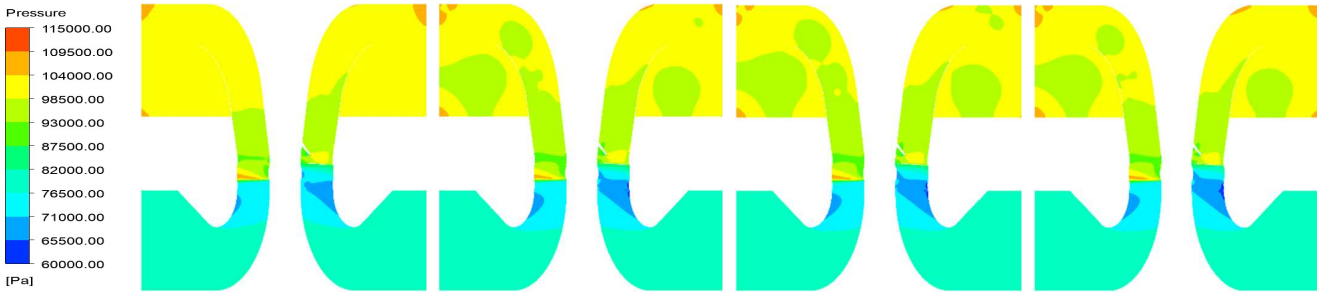

(**a**) d = 1 mm (**b**) d = 2.5 mm (**c**) d = 3.5 mm (**d**) d = 5 mm

Figure 8. Pressure distribution of the Z–X section under the design conditions.

As shown in Figure 9, due to the existence of the tip clearance, there was a significant backflow at the top of the impeller blade, flow around the outlet, flow pattern disorder and so on. The flow entered the impeller, and with the increase in tip clearance, the backflow in the impeller channel increased significantly. When the clearance was small, the leakage was small, resulting in a large pressure difference on both sides of the blade, which led to the formation of a flow vortex in the impeller passage. With the gradual increase in the tip clearance, the leakage increased, causing part of the fluid gathered in the working face to cross the clearance to form backflow. The larger the clearance was, the more backflow there was. By observing the above figure, it can be seen that the backflow caused by a certain gap (Figure 9b) could make the fluid flow smoother, which was sufficient to demonstrate that a certain gap (Figure 9b) could improve the flow pattern of the impeller channel.

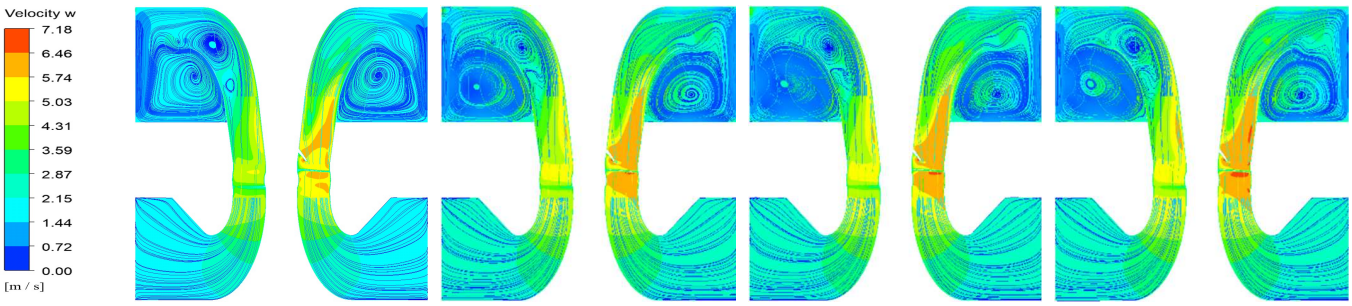

(**a**) d = 1 mm (**b**) d = 2.5 mm (**c**) d = 3.5 mm (**d**) d = 5 mm

Figure 9. Velocity distribution of the Z-X section under the design conditions.

3.5. Influence of Clearance Change on Tip Leakage of Clearance Layer

Figures 10 and 11 show the relative velocity vectors and leaky vortex 3D shapes under different tip clearances at a $0.6Q_0$ flow rate. When the tip clearance was 1 mm, the leakage of the tip head relative to other positions was large and the pressure difference between the

working face and the back of the blade was also the largest. Since the tip clearance was very small relative to the impeller diameter and the collision between the leakage flow and the pump shell caused loss, the actual leakage flow was a small part relative to the mainstream and had little effect on the flow. Under the influence of the mainstream after the formation of the leakage flow, the leakage flow was mixed into the mainstream. The pump device had good performance under this small tip clearance.

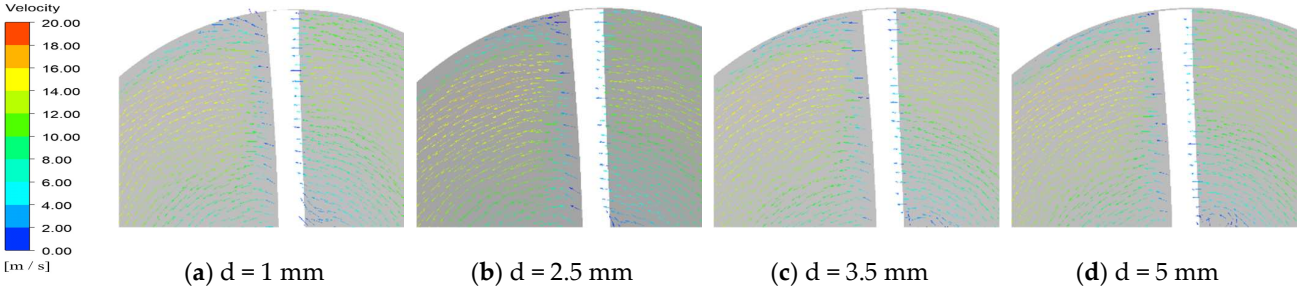

(**a**) d = 1 mm (**b**) d = 2.5 mm (**c**) d = 3.5 mm (**d**) d = 5 mm

Figure 10. Relative velocity vector diagram under the $0.6Q_0$ flow condition.

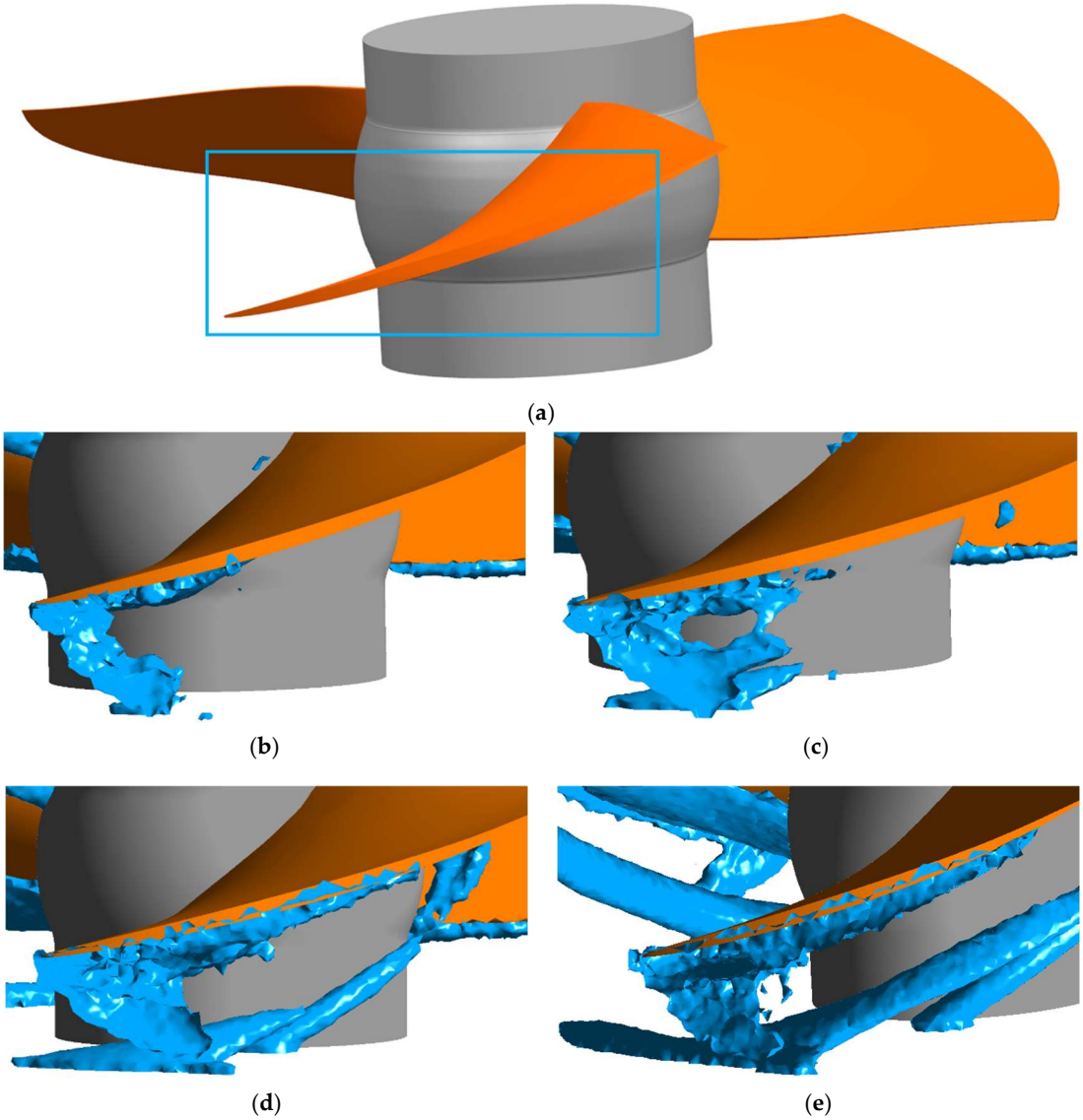

(**a**)

(**b**) (**c**)

(**d**) (**e**)

Figure 11. Leaky vortex 3D shape. (**a**) Observation angle; (**b**) d = 1 mm; (**c**) d = 2.5 mm; (**d**) d = 3.5 mm; (**e**) d = 5 mm.

As the tip clearance gradually increased, the leakage also gradually increased. Compared with Figure 11a, a relatively obvious leakage flow was formed in Figure 11b. At this time, the influence of the leakage flow on the mainstream also increased, but the leakage flow at this time was still relatively small and was still mixed into the mainstream, and thus, the leakage vortex disappeared. As the tip clearance was further expanded to 5 mm, the leakage volume was further increased and the leakage vortex intensified. The leakage flow and the mainstream had a certain ability to resist and interact. In the encounter position, the entrainment phenomenon occurred, resulting in the intensification of the vortex in the flow channel. At this time, the larger tip clearance had a negative impact on the performance of the pump device and caused concomitant damage to the blade.

3.6. Characteristics of the Pressure Pulsation in the Tip Clearance Region

In order to further reveal the influence of the tip clearance on the flow characteristics in the rim area of the vertical axial flow pump under the design conditions, the time domain and frequency domain characteristics were analyzed by monitoring the pressure pulsation characteristics in the tip clearance area. The amplitude of the pressure pulsation was described by the relative value of the double-amplitude peak-to-peak value of the mixing frequency in the time domain, and the spectral characteristics of the pressure pulsation were obtained by using the fast Fourier transform (FFT). In order to improve the frequency resolution of the FFT analysis, the sampling time was continuously calculated for four cycles, starting from the fourth impeller rotation cycle, and the static pressure data of the monitoring points in these four cycles were collected to analyze the flow field spectrum. The amplitude of the pressure pulsation was represented by the pressure pulsation coefficient Cp, which is expressed as follows:

$$C_p = \frac{\Delta P}{0.5\rho U^2}$$

where

$$U = \frac{\pi n D}{60}$$

In these formulae, ΔP is the difference between the instantaneous pressure and the average static pressure at the monitoring point (Pa); ρ is the fluid density (kg/m^3); D is the impeller diameter (m); U is the peripheral speed (m/s) and n is the pump speed (r/min).

Table 3 is the amplitude table of the monitoring points at the impeller under different tip clearances. From the data shown in this table, it can be seen that the main frequency of the monitoring points at the impeller was a multiple of the rotational frequency of the impeller. Because of the influence of the periodic rotation of the three blades of the impeller and the mutual interference of the static flow field at the inlet, the main frequency of most of the monitoring points at the impeller was the same as the blade frequency. In particular, the main frequency of the measuring points at the impeller rim and the inlet hub was the blade frequency. The outlet of the impeller was connected to the inlet of the guide vane; therefore, in addition to being affected by the main frequency of the impeller, some frequencies were also affected by the guide vane. Under different tip clearances, with the increase in the clearance, the amplitude first increased and then decreased, while the change trend of the position of the inlet and outlet and the axial monitoring position was basically the same; therefore, the three points at the rim were further analyzed.

Figure 12 shows the pressure pulsation characteristics of the monitoring point P3 near the impeller inlet for different tip clearances. It can be seen that the pressure pulsation at the monitoring point of the pressure pulsation at the impeller inlet had a relatively obvious law, which was similar to a sinusoidal waveform. There was a complete peak and trough in one cycle. When the tip clearance was small, the pressure variation range was large because the impact of the leakage flow was large under the same working conditions. When the tip clearance was small, there were many complex high-frequency components in the frequency domain. Since P3 was located at the leading edge of the tip, the pressure

here was affected by the direct work done by the blade and also by the leakage flow, which caused the flow here to be more stable. It was complicated and exacerbated the instability of the flow.

Table 3. Amplitudes of the monitoring points at the impeller when the clearances were 1, 2.5, 3.5 and mm.

Location	Point Number	Main Frequency (Hz)	Amplitude
Three points of impeller rim clearance	P1	2.5	0.00345
	P2	2.5	0.00683
	P3	5.0	0.00817
Circumferential three points of impeller inlet	P4	7.5	0.00345
	P5	2.5	0.00393
	P6	2.5	0.00631
Three axial points at the impeller rim	P7	2.5	0.00540
	P8	2.5	0.00271
	P9	17.5	0.00340
Circumferential three points of impeller outlet	P10	7.5	0.00715
	P11	17.5	0.00928
	P12	17.5	0.01403
Three points of impeller rim clearance	P1	2.5	0.00322
	P2	2.5	0.00689
	P3	2.5	0.01339
Circumferential three points of impeller inlet	P4	7.5	0.00259
	P5	2.5	0.00390
	P6	2.5	0.00655
Three axial points at the impeller rim	P7	2.5	0.00556
	P8	2.5	0.00223
	P9	17.5	0.00381
Circumferential three points of impeller outlet	P10	7.5	0.00800
	P11	7.5	0.01643
	P12	17.5	0.01342
Three points of impeller rim clearance	P1	2.5	0.00374
	P2	2.5	0.00733
	P3	2.5	0.01285
Circumferential three points of impeller inlet	P4	7.5	0.00285
	P5	2.5	0.00406
	P6	2.5	0.00664
Three axial points at the impeller rim	P7	2.5	0.00571
	P8	2.5	0.00233
	P9	17.5	0.00376
Circumferential three points of impeller outlet	P10	7.5	0.00834
	P11	7.5	0.01673
	P12	17.5	0.01316
Three points of impeller rim clearance	P1	2.5	0.00395
	P2	2.5	0.00751
	P3	2.5	0.01189

Table 3. *Cont.*

Location	Point Number	Main Frequency (Hz)	Amplitude
Circumferential three points of impeller inlet	P4	7.5	0.00290
	P5	2.5	0.00402
	P6	2.5	0.00627
Three axial points at the impeller rim	P7	2.5	0.00553
	P8	2.5	0.00234
	P9	17.5	0.00364
Circumferential three points of impeller outlet	P10	7.5	0.00848
	P11	7.5	0.01679
	P12	17.5	0.01257

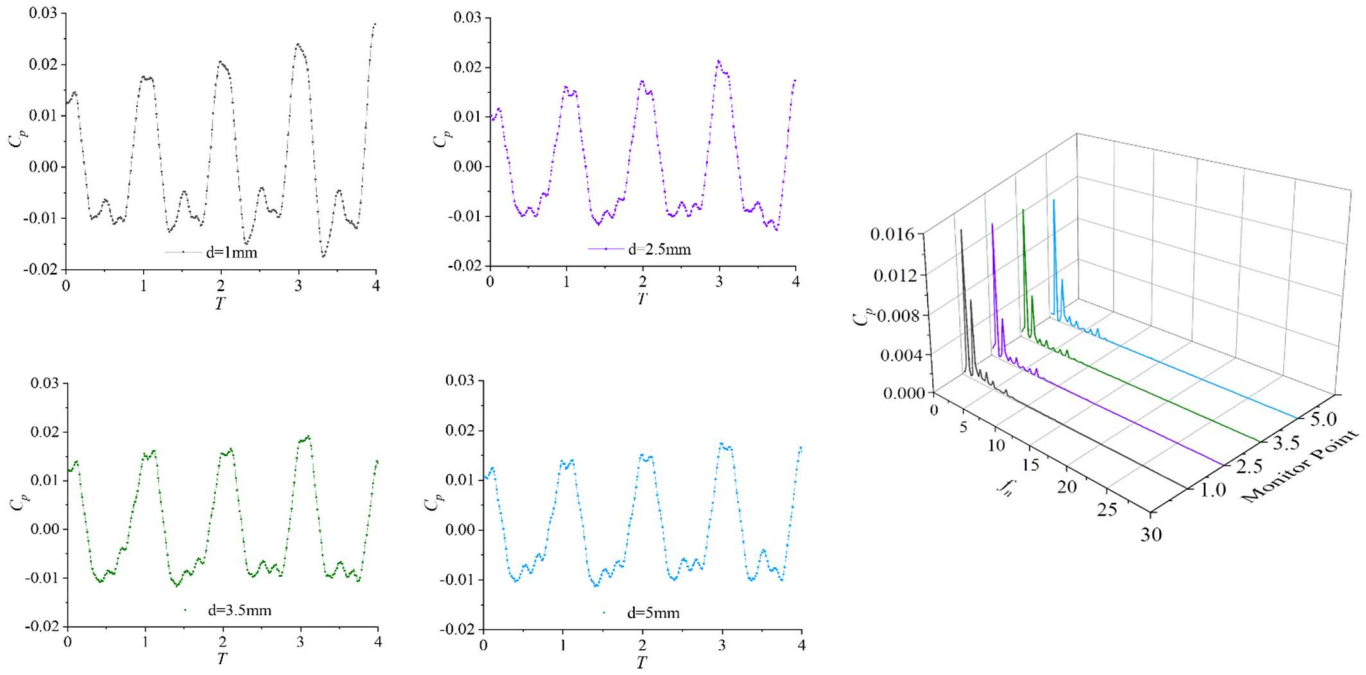

(**a**) Time domain diagram (**b**) Frequency domain plot

Figure 12. Pressure pulsation characteristics of the tip inlet edge point P3.

Figure 13 shows the pressure pulsation characteristics of the monitoring point P2 in the middle of the blade tip. It can be seen that the four different blade tip clearances showed similar regular changes, but the amplitudes were slightly different; its frequency domain characteristics also had complex components, but they were not as chaotic as the inlet end, and the middle of the blade tip was affected by the periodic rotation of the blade and leakage flow.

Figure 14 shows the pressure pulsation characteristics of the monitoring point P1 at the tip outlet. It can be seen that the regularity was not as obvious as before in the case of different tip clearances since there were no obvious periodic peaks and valleys, showing a certain amount of randomness; its frequency domain also had a large number of high-frequency parts, but it was not as good as the inlet and the middle of the tip, and as the tip clearance increased, the high-frequency part decreased, which was caused by interference from the leakage flow.

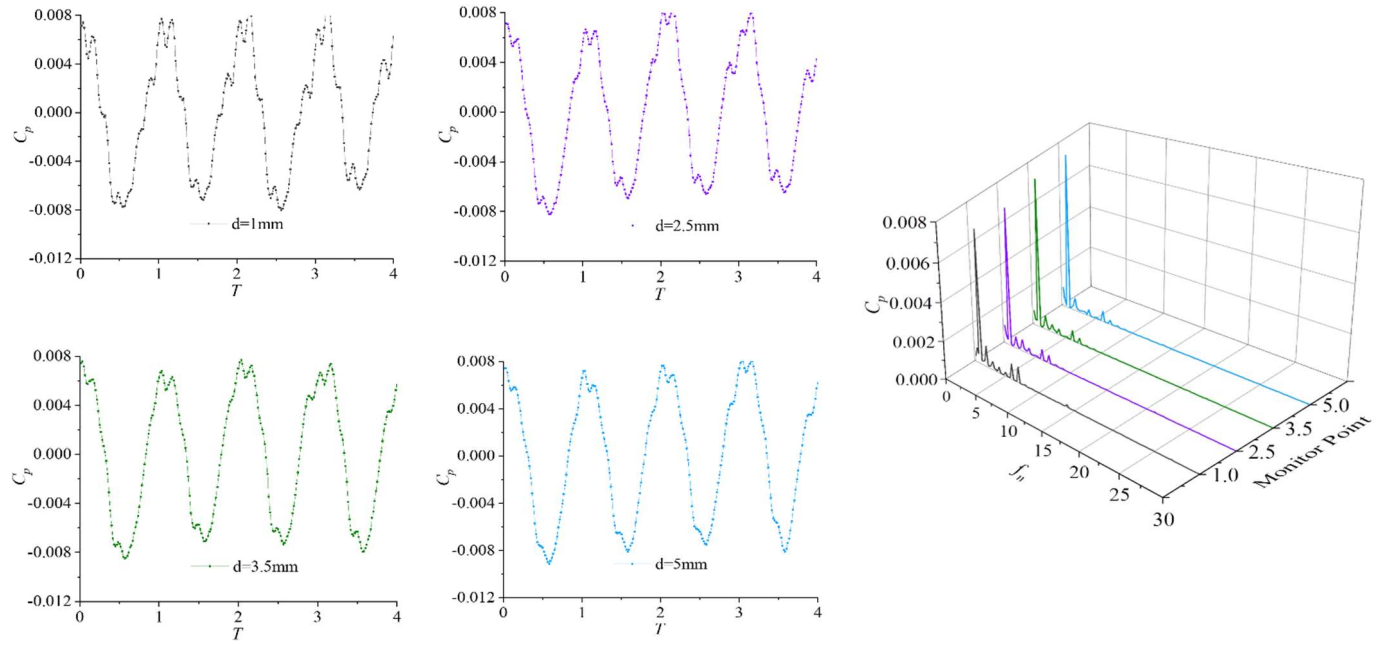

(**a**) Time domain diagram (**b**) Frequency domain plot

Figure 13. Pressure pulsation characteristics at point P2 in the middle of the blade tip.

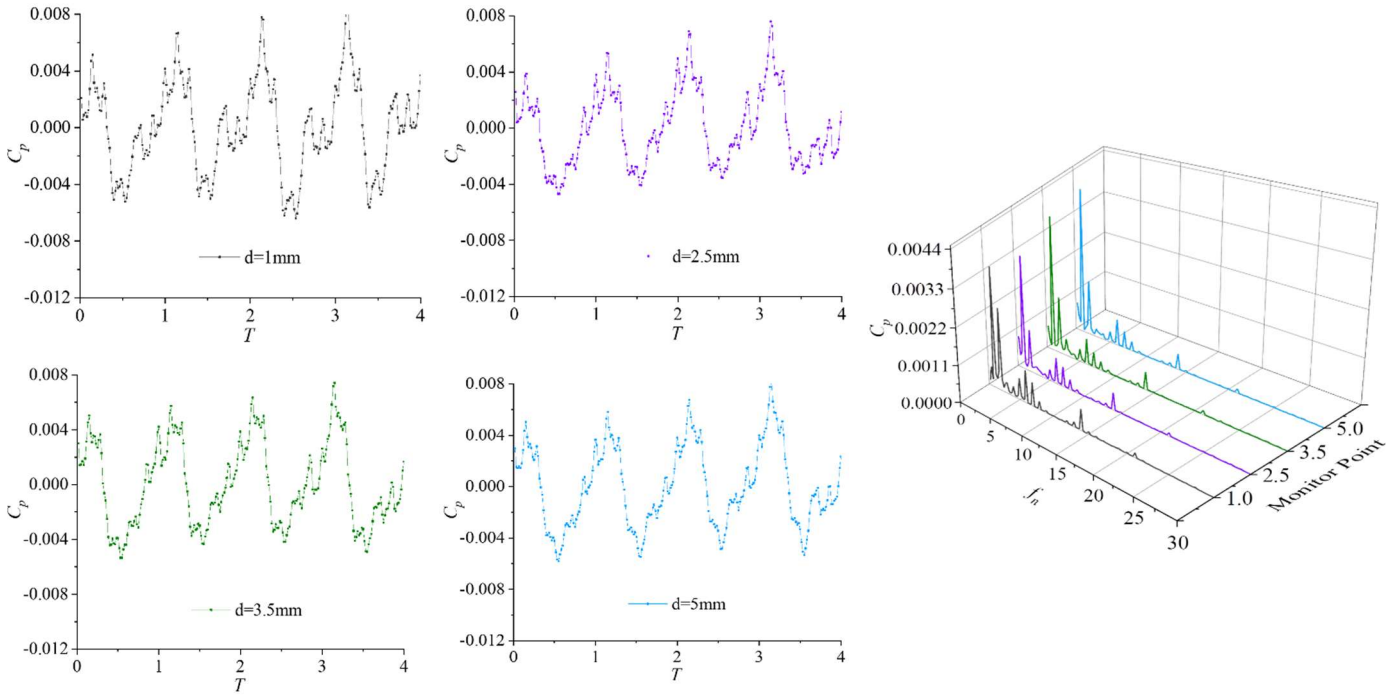

(**a**) Time domain diagram (**b**) Frequency domain plot

Figure 14. Pressure pulsation characteristics of the tip outlet edge point P1.

4. Conclusions

(1) As the tip clearance increased, the lift and efficiency decreased, but there was no linear relationship between the degree of the decrease and the change in the clearance. Furthermore, in the process of increasing the flow rate, the difference in the head under the size of the tip clearance first decreased and then increased, but the difference in the

head under the condition of a small flow was larger than that under the condition of a large flow. In the relationship between the efficiency and flow rate, from a small flow condition to a large flow condition, the efficiency first increased and then decreased, forming a saddle region, and the pump performance dropped sharply after the flow rate exceeded the design condition.

(2) In the Z–X section, there was an obvious backflow at the top of the impeller blade, and there was a flow around the outlet and flow pattern disorder. When the gap value was 2.5 mm, a certain amount of reflux caused the fluid flow to be smoother, indicating that a certain gap could improve the flow pattern of the channel.

(3) Under different tip clearance values, the variation trend of the pressure in the impeller was basically the same. However, the pressure fluctuation changed obviously at the flange clearance, and the pressure fluctuation amplitude was from 0.00322 to 0.01339.

(4) The pressure pulsation characteristics showed that the axial flow pump showed strong unsteady characteristics under the design conditions. The leakage flow caused by the tip clearance aggravated the flow instability and had a significant impact on the pressure pulsation characteristics in the clearance area.

Author Contributions: Data curation, L.C.; Formal analysis, J.S.; Methodology, F.X. and W.P.; Writing—original draft, J.S. and J.L.; Writing—review and editing, L.C., J.S., Y.G. and J.Z.; Supervision, L.C. All authors have read and agreed to the published version of the manuscript.

Funding: This research was funded by the National Natural Science Foundation of China (grant no. 51779214), a project funded by the Priority Academic Program Development of Jiangsu Higher Education Institutions (PAPD), the Key Project of Water Conservancy in Jiangsu Province (grant no. 2020030 and 2020027) and the Jiangsu Province South-to-North Water Transfer Technology Research and Development Project (SSY-JS-2020-F-45).

Institutional Review Board Statement: Not applicable.

Informed Consent Statement: Not applicable.

Data Availability Statement: Data on the analysis and reporting results during the study can be obtained by contacting the authors.

Acknowledgments: The authors thank the College of Hydraulic Science and Engineering, Yangzhou University. The author is very grateful for the discussions with Li Cheng and Jiao Weixuan. A huge amount of thanks is due to the editor and reviewers for their valuable comments to improve the quality of this paper.

Conflicts of Interest: The authors declare no conflict of interest.

References

1. Lu, X.; Tong, H.; Feng, J. Improvement of the influent flow state of the intake pool of the urban water pumping station. *Drain. Irrig. Mach.* **2007**, *25*, 24–28. (In Chinese) [CrossRef]
2. Hu, X.; Liu, J.; Wu, J.; Ma, Q. Analysis of the impact of drainage from the pumping stations along the middle and lower reaches of the Yangtze River on the flood control of the mainstream. *People's Yangtze River* **2020**, *51*, 172–178. (In Chinese) [CrossRef]
3. Liu, C. Analysis of technological innovation and development of axial flow pump system. *J. Agric. Mach.* **2015**, *46*, 49–59. (In Chinese) [CrossRef]
4. Zhao, C. Overview of the South-to-North Water Diversion Project. *Water Conserv. Constr. Manag.* **2021**, *41*, 5–9. (In Chinese) [CrossRef]
5. Mondal, P.; Mukherjee, S. A New Analytical Approach to Predict the Operating Point of a Pumping System Having Groups of Different Types of Radial-Flow Pumps in Parallel and the Resulting Flow Division in the Piping Network. *J. Inst. Eng.* **2012**, *93*, 83–91. [CrossRef]
6. Xie, K. Analysis of the status quo of real-time operation status assessment technology of pumping stations. *Think Tank Times* **2018**, *48*, 199+204. (In Chinese)
7. Zhang, D.; Shen, X.; Dong, Y.; Wang, C.; Liu, A.; Shi, W. Numerical simulation of internal flow characteristics of oblique flow pumps with different tip clearances. *Chin. J. Drain. Irrig. Mech. Eng.* **2020**, *38*, 757–763. (In Chinese) [CrossRef]
8. Shi, W.; Zhang, H.; Chen, B.; Zhang, D.; Zhang, L. Numerical calculation of the internal flow field of an axial flow pump with different tip clearances. *Chin. J. Drain. Irrig. Mech. Eng.* **2010**, *28*, 374–377+406. (In Chinese)

9. Zhang, Q.; Yang, J.; Li, H.; Yan, S.; Li, Y. Research on flow characteristics of variable tip clearance in semi-open impeller centrifugal pump. *Hydraul. Pneum. Seal.* **2021**, *41*, 6. (In Chinese)
10. Li, H.; Su, X.; Yuan, X. Research on turbulent characteristics of tip clearance flow based on DDES simulation. *J. Eng. Thermophys.* **2021**, *42*, 342–348. (In Chinese)
11. Lu, J.; Guo, L.; Wang, L.; Wang, W.; Guo, P.; Luo, X. Research on unsteady flow characteristics of tip clearance of half-open impeller centrifugal pump. *J. Agric. Mach.* **2019**, *50*, 163–172. (In Chinese) [CrossRef]
12. Li, Z.; He, F.; Pan, S. Internal flow analysis of tubular turbine blade tip clearance under partial working conditions. *Therm. Power Eng.* **2021**, *36*, 16–23. (In Chinese) [CrossRef]
13. Liu, Y.; Tan, L.; Hao, Y. Energy performance and flow patterns of a mixed-flow pump with different tip clearance sizes. *Energies* **2017**, *10*, 191. [CrossRef]
14. Kan, N.; Liu, Z.; Shi, G. Effect of Tip Clearance on Helico-Axial Flow Pump Performance at Off-Design Case. *Processes* **2021**, *9*, 1653. [CrossRef]
15. Shen, S.; Qian, Z.; Ji, B. Numerical investigation of tip flow dynamics and main flow characteristics with varying tip clearance widths for an axial-flow pump. *Proc. Inst. Mech. Eng. Part A J. Power Energy* **2019**, *233*, 476–488. [CrossRef]
16. Feng, J.; Luo, X.; Guo, P. Influence of tip clearance on pressure fluctuations in an axial flow pump. *J. Mech. Sci. Technol.* **2016**, *30*, 1603–1610. [CrossRef]
17. Li, Y.; Bi, Z.; Li, R.; Hu, P. Numerical analysis of pressure pulsation characteristics of oblique flow pump with different tip clearances. *J. Hydraul. Eng.* **2015**, *46*, 497–504. (In Chinese) [CrossRef]
18. Zhang, H.; Chen, B.; Wang, B.; Shi, C.; Shen, D. Effect of tip clearance on internal pressure pulsation of screw centrifugal pump. *Chin. J. Agric. Eng.* **2017**, *33*, 84–89. (In Chinese) [CrossRef]
19. Li, R.; Hu, P.; Li, Y.; Bi, Z.; Zhou, D. Numerical analysis of the influence of blade tip clearance on inlet pressure pulsation of oblique flow pump. *Chin. J. Drain. Irrig. Mech. Eng.* **2015**, *33*, 560–565. (In Chinese) [CrossRef]
20. Li, Y.; Shen, J.; Hong, Y.; Liu, Z. Numerical prediction of the influence of blade tip clearance on pressure pulsation of axial flow pump rim. *J. Agric. Mach.* **2014**, *45*, 59–64+58. (In Chinese) [CrossRef]
21. Guelich, J. Effect or Reynolds Number and Surface Roughness on the Efficiency of Centrifugal Pumps. *J. Fluids Eng.* **2003**, *125*, 670–679. [CrossRef]
22. Ulanicki, B.; Kahler, J.; Coulbeck, B. Modeling the Efficiency and Power Characteristics of a Pump Group. *J. Water Resour. Plan. Manag.* **2008**, *134*, 88–93. [CrossRef]
23. Shi, L.; Zhang, W.; Jiao, H.; Tang, F.; Wang, L.; Sun, D.; Shi, W. Numerical simulation and experimental study on the comparison of the hydraulic characteristics of an axial-flow pump and a full tubular pump. *Renew. Energy* **2020**, *153*, 1455–1464. [CrossRef]
24. Nm, A.; Gk, A.; Dh, A. A real-time energy management strategy for pumped hydro storage systems in farmhouses—ScienceDirect. *J. Energy Storage* **2020**, *32*, 101928. [CrossRef]
25. Luna, T.; Ribau, J.; Figueiredo, D. Improving energy efficiency in water supply systems with pump scheduling optimization. *J. Clean. Prod.* **2019**, *213*, 342–356. [CrossRef]
26. Shi, L.; Zhu, J.; Tang, F.; Wang, C. Multi-Disciplinary Optimization Design of Axial-Flow Pump Impellers Based on the Approximation Mode. *Energies* **2020**, *13*, 779. [CrossRef]
27. Yang, Y.; Zhou, L.; Bai, L.; Xu, H.; Lv, W.; Shi, W.; Wang, H. Numerical Investigation of Tip Clearance Effects on the Performance and Flow Pattern Within a Sewage Pump. *J. Fluids Eng.* **2022**, *144*, 081202. [CrossRef]
28. Zhang, D.; Wu, S.; Shi, W. Application and verification of different turbulence models in eddy simulation of axial flow pump tip leakage. *Chin. J. Agric. Eng.* **2013**, *13*, 46–53. (In Chinese) [CrossRef]